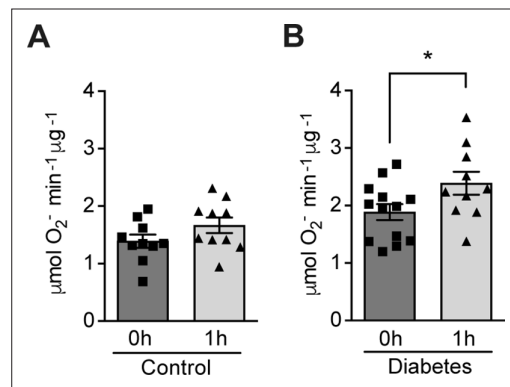


---

## Figures and figure supplements

Repression of hypoxia-inducible factor-1 contributes to increased mitochondrial reactive oxygen species production in diabetes

**Xiaowei Zheng *et al***



**Figure 1.** Hypoxia increases circulating ROS in patients with diabetes but not in control subjects without diabetes. Healthy controls (**A**) and subjects with type 1 diabetes (**B**) were exposed to intermittent hypoxia for 1 hr. Peripheral blood was taken before (0h) and after (1h) hypoxia exposure. ROS levels were analyzed using Electron Paramagnetic Resonance (EPR) Spectroscopy with CPH spin probes (n = 10–13). Data are represented as mean ± SEM. \*, p < 0.05 analysed using unpaired two-sided Student's t-test. This figure has one figure supplement. Source data are shown in **Figure 1—source data 1**.

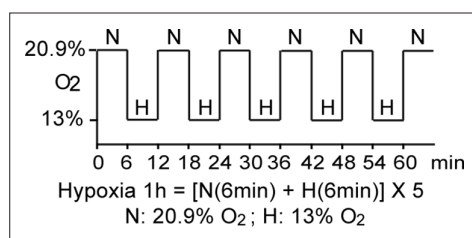


**Figure 1—figure supplement 1.** Schematic demonstration of hypoxia exposure protocol in the clinical study. The study participants were exposed to intermittent hypoxia for 1 hr, consisting of five hypoxic episodes (H, 13% O<sub>2</sub>, 6 min) that alternate with normoxic episodes (N, 20.9% O<sub>2</sub>, 6 min).

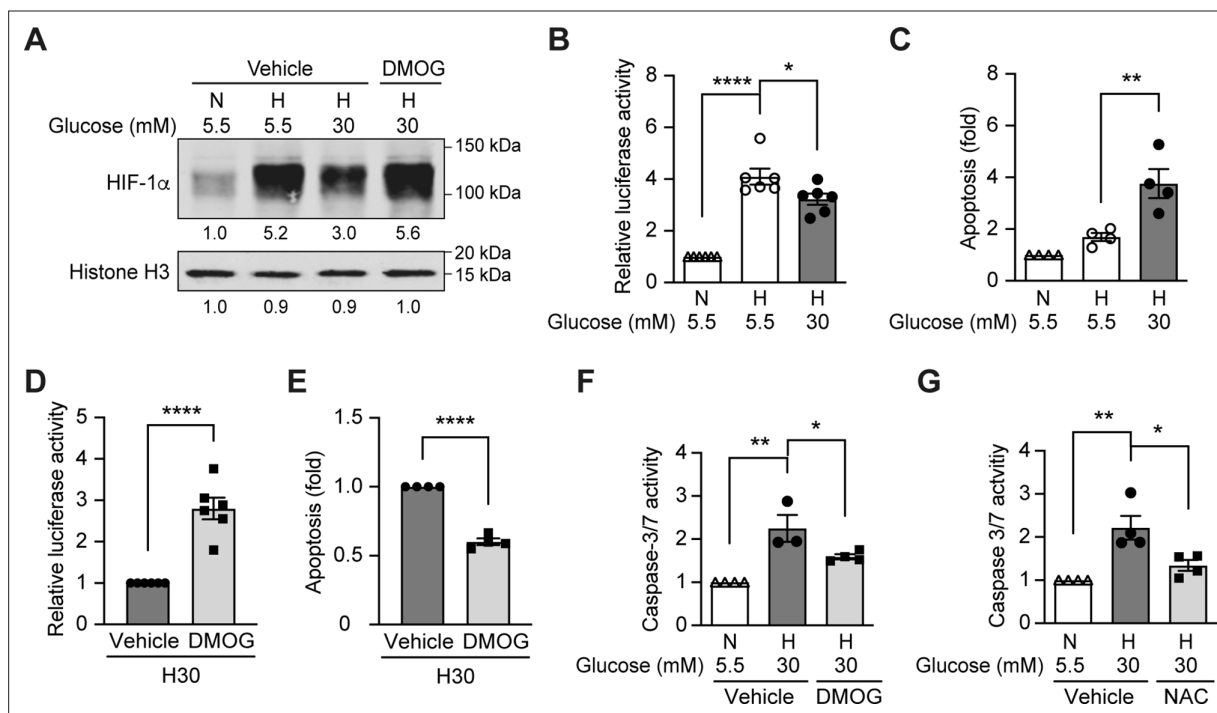


**Figure 2.** High glucose levels inhibit HIF-1 signaling and induce apoptosis, which can be rescued by PHD inhibitor DMOG. (A) mIMCD-3 cells were cultured in normal (5.5 mM) or high (30 mM) glucose media in the presence of DMOG or vehicle for 24 hr, and were exposed to hypoxia (H) or normoxia (N) for 6 hr before harvest. The nuclear expression of HIF-1 $\alpha$  and Histone H3 was measured using western blotting. (B–F) mIMCD-3 cells were exposed to 5.5 or 30 mM glucose levels in normoxia (N) or hypoxia (H) in the presence or absence of DMOG or vehicle for 24 hr. The relative HRE-driven luciferase activity (B and D,  $n = 6$ ), apoptosis (C and E,  $n = 4$ ), and the caspase 3/7 activity (F,  $n = 3–4$ ) were assessed. (G) Caspase 3/7 activity was evaluated in mIMCD-3 cells that were pre-treated with 1 mM NAC or vehicle for 1 hr before exposure to 5.5 or 30 mM glucose levels in normoxia (N) or hypoxia (H) for 24 hr ( $n = 4$ ). The data under control conditions were considered as 1.0. Data are shown as mean  $\pm$  SEM. \*,  $p < 0.05$ ; \*\*,  $p < 0.01$ ; \*\*\*,  $p < 0.001$ ; \*\*\*\*,  $p < 0.0001$  using one-way ANOVA followed by Bonferroni's post hoc test (B–C, F–G), and unpaired two-sided Student t-test (D–E). This figure has one figure supplement. Source data are shown in **Figure 2—source data 1**.

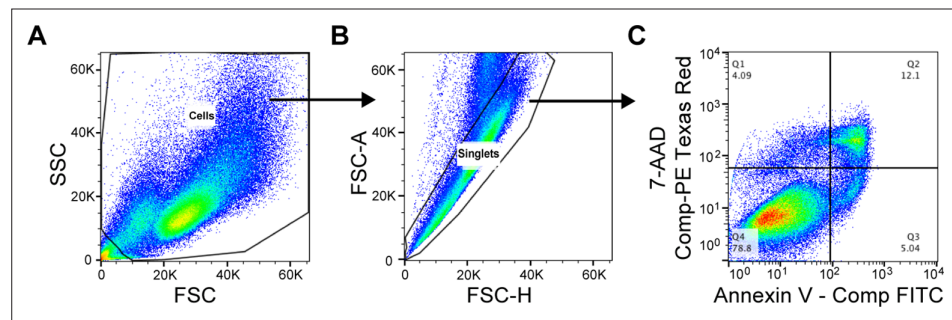


**Figure 2—figure supplement 1.** Flow cytometry gating strategy for the evaluation of cellular apoptosis. Compensation controls were performed prior to flow analysis. (A) Cell population was defined based on FSC / SSC. (B) Single cells were gated based on FSC-H / FSC-A. (C) The Annexin V – positive and 7-AAD – negative apoptotic cell population is shown in Quadrant 3 (Q3) of the bivariate histogram based on the compensated intensity of Annexin V – FITC and 7-AAD – PE Texas Red.

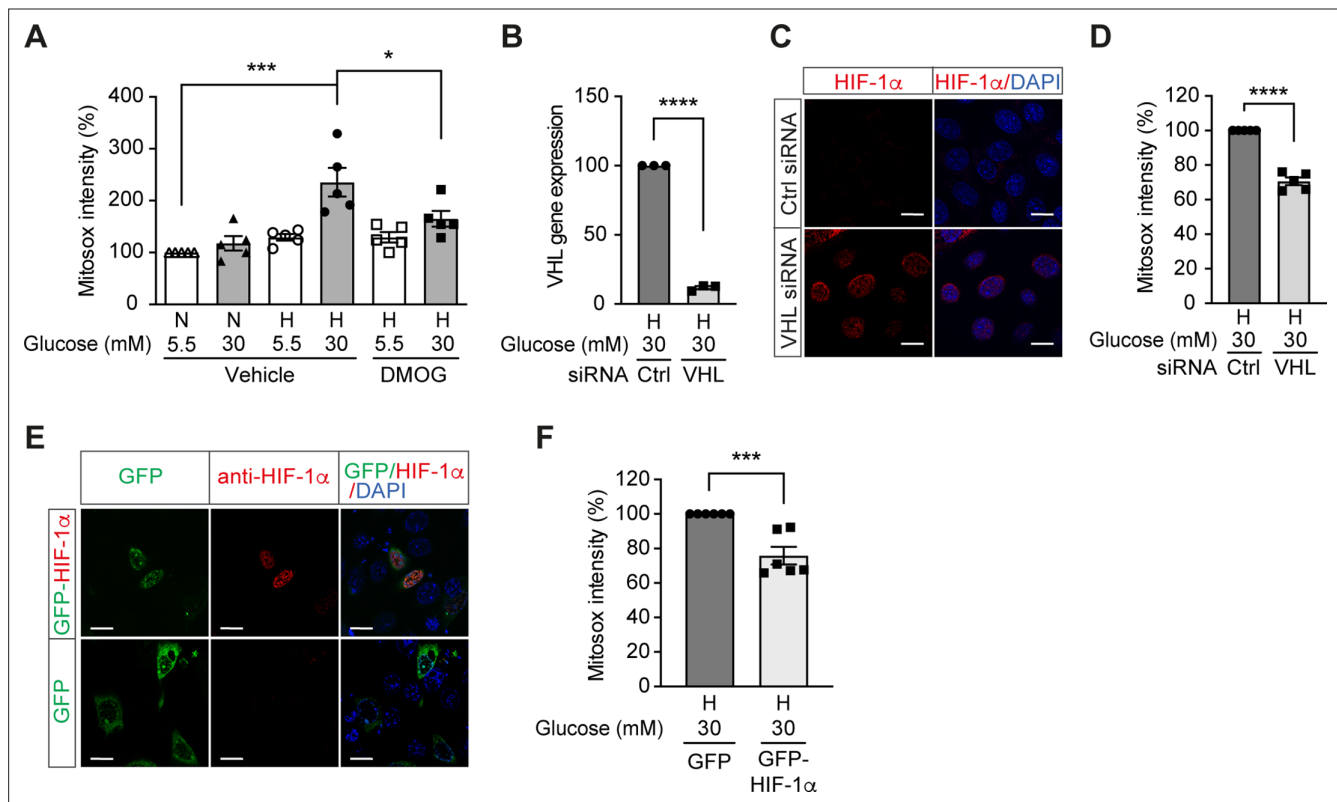


**Figure 3.** High glucose levels induce mitochondrial ROS overproduction in hypoxia, which can be rescued by promoting HIF-1 function. **(A)** Mitochondrial ROS levels were measured as mitosox intensity in mIMCD-3 cells cultured in normal (5.5 mM) or high (30 mM) glucose media in normoxia (N) or hypoxia (H) for 24 hr in the presence of DMOG or vehicle ( $n = 5$ ). **(B–D)** mIMCD-3 cells were transfected with von Hippel–Lindau tumour suppressor (VHL) or control (Ctrl) siRNA, and exposed to hypoxia (H) and 30 mM glucose for 24 hr. VHL gene expression **(B)**, endogenous HIF-1 $\alpha$  expression (red) and DAPI staining (blue) **(C)** and mitochondrial ROS levels **(D)**,  $n = 5$  were assessed using quantitative RT-PCR, fluorescent immunocytochemistry and flow cytometry, respectively. **(E and F)** mIMCD-3 cells were transfected with plasmids encoding GFP or GFP-HIF-1 $\alpha$ , and exposed to hypoxia and 30 mM glucose for 24 hr. **(E)** Expression of GFP and GFP-HIF-1 $\alpha$  (green) were detected using confocal microscopy. The nuclear HIF-1 $\alpha$  expression was confirmed by immunocytochemistry using anti-HIF-1 $\alpha$  antibody (red). Nuclei were stained blue with DAPI. **(F)** Mitochondrial ROS levels are shown ( $n = 6$ ). The mitosox intensity of cells cultured under control conditions were considered as 100%. Data are shown as mean  $\pm$  SEM. \*,  $p < 0.05$ ; \*\*\*,  $p < 0.001$ ; \*\*\*\*,  $p < 0.0001$  using one-way ANOVA followed by Bonferroni's post hoc test **(A)**, and unpaired two-sided Student t-test **(B, D and F)**. This figure has two figure supplements. Source data are shown in **Figure 3—source data 1**. Scale bar: 50  $\mu$ m.

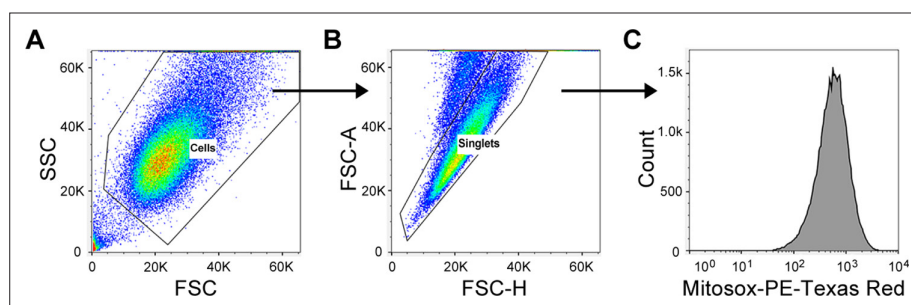


**Figure 3—figure supplement 1.** Flow cytometry gating strategy for the evaluation of mitox intensity. (A) Cell population was defined based on FSC / SSC. (B) Single cells were gated based on FSC-H / FSC-A. (C) Mitox-PE-Texas red intensity was evaluated among single cells.

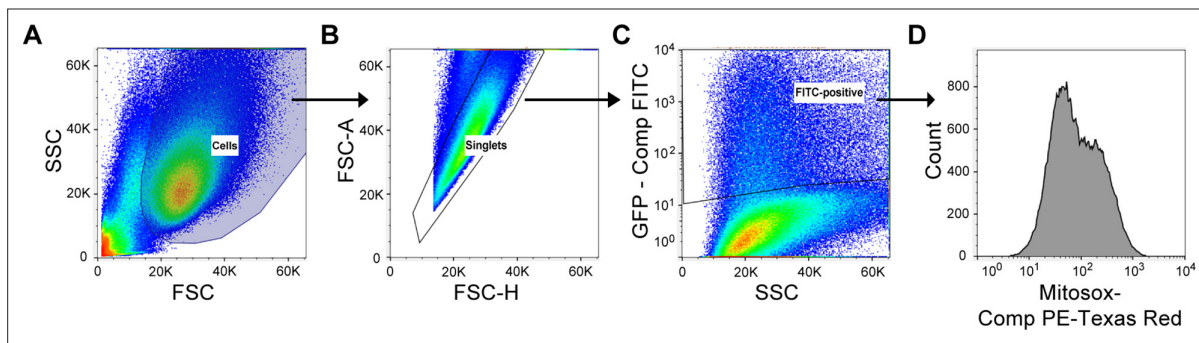


**Figure 3—figure supplement 2.** Flow cytometry gating strategy for the evaluation of mitox intensity in mIMCD3 cells transfected with plasmids encoding GFP or GFP-fused protein. Compensation controls were performed prior to flow analysis. **(A)** Cell population was defined based on FSC/SSC. **(B)** Single cells were gated based on FSC-H/FSC-A. **(C)** GFP-expressing (compensated (comp) FITC-positive) cells were gated among single cells. **(D)** Mitox-PE-Texas red (compensated) intensity was evaluated among GFP-expressing (FITC-positive) cells.



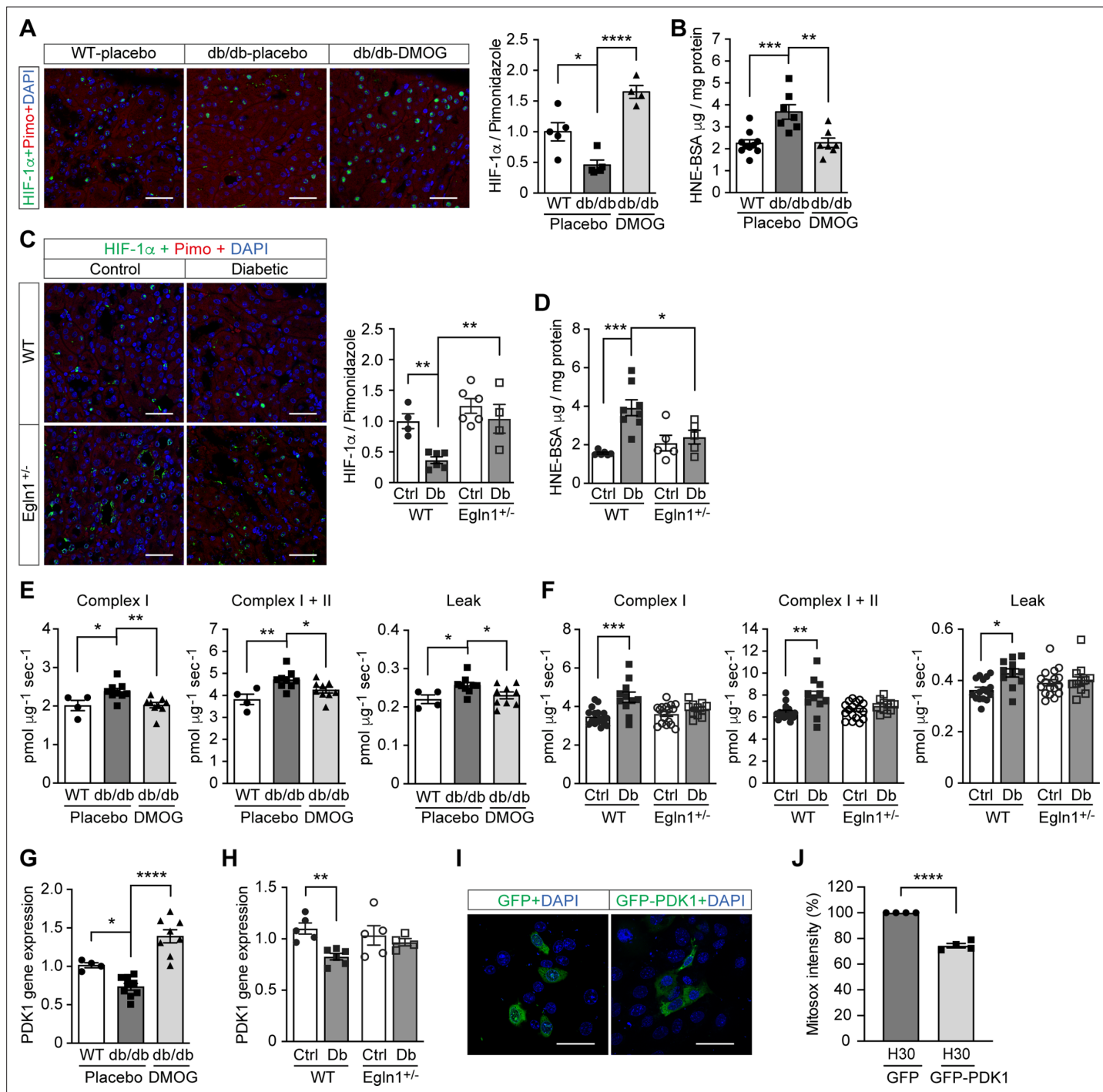


**Figure 4.** Promoting HIF-1 function attenuates renal ROS excess and mitochondrial respiration in mouse models of diabetes. Kidneys were harvested from wild-type (WT) and *Lep<sup>db/db</sup>* diabetic mice (db/db) that were treated with placebo (vehicle) or DMOG (**A–B, E, G**), and from non-diabetic control (Ctrl) or diabetic (Db) wild-type (WT) and *EglN1<sup>+/-</sup>* mice (**C–D, F, H**). (**A and C**) HIF-1α (green), pimonidazole (red, hypoxia marker) and DAPI (blue, nuclear staining) signals were detected by fluorescent immunohistochemistry, and relative HIF-1α expression levels were quantified (**A**, n = 4–5; **C**, n = 4–6). Scale bar: 100 μm. (**B and D**) Renal ROS levels were detected using the OxiSelect HNE adduct competitive ELISA kit (**B**, n = 7–10; **D**, n = 5–8). (**E and F**) Mitochondrial respiratory function was evaluated using high resolution respirometry (**E**, n = 4–9; **F**, n = 11–17). (**G and H**) PDK1 gene expression in kidneys (**G**, n = 4–9; **H**, n = 4–6). (**I and J**) mIMCD-3 cells were transfected with plasmids encoding GFP or GFP-PDK1, and exposed to hypoxia and 30 mM glucose (H30) for 24 hr. (**I**) Expression of GFP and GFP-HIF-1α (green) and nuclear DAPI staining (blue) were detected using confocal microscopy. Scale bar: 50 μm. (**J**) Mitochondrial ROS levels are shown (n = 4). Data are shown as mean ± SEM. \*, p < 0.05; \*\*, p < 0.01; \*\*\*, p < 0.001; \*\*\*\*, p < 0.0001 using one-way ANOVA (**A, B, E, G**) and two-way ANOVA (**C, D, F, H**) followed by multi-comparison post hoc tests, and unpaired two-sided Student t-test (**J**). This figure has three figure supplements. Source data are shown in **Figure 4—source data 1**.

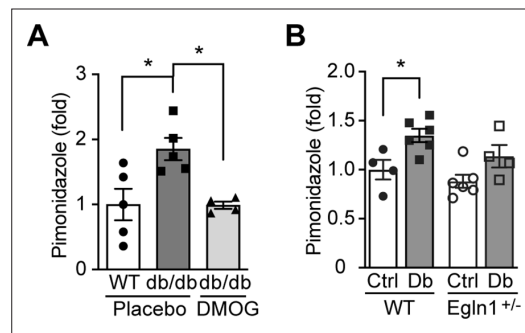


**Figure 4—figure supplement 1.** Kidney in diabetes is more hypoxic. Pimonidazole (60 mg/kg body weight) was *i.p.* administered to mice 90 min prior to tissue harvest from wild-type (WT) and *Lepr<sup>db/db</sup>* diabetic mice (db/db) that were treated with placebo (vehicle) or DMOG (**A**), and from non-diabetic control (Ctrl) or diabetic (Db) wild-type (WT) and *EglN1<sup>+/-</sup>* mice (**B**). Pimonidazole adducts were detected on kidney sections using fluorescent immunohistochemistry and fold induction of pimonidazole signal is shown. \*,  $p < 0.05$  using one-way ANOVA (**A**) and two-way ANOVA (**B**) followed by multi-comparison post hoc tests. Source data are shown in **Figure 4—figure supplement 1—source data 1**.

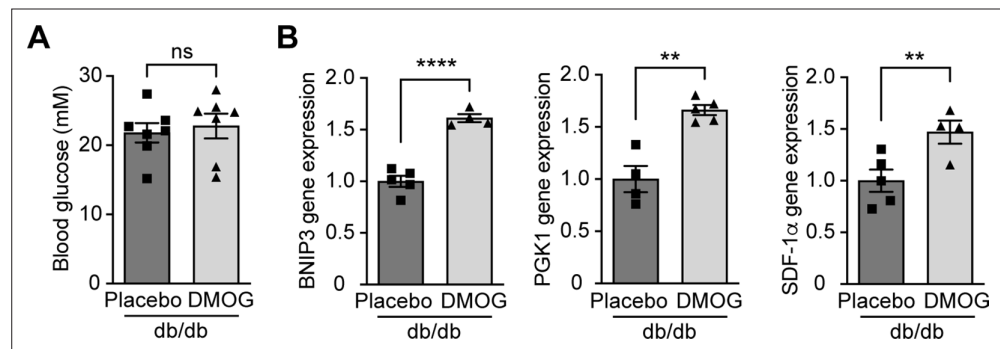


**Figure 4—figure supplement 2.** DMOG increases HIF-1 target gene expression in *Lepr<sup>db/db</sup>* mice without affecting blood glucose levels. *Lepr<sup>db/db</sup>* diabetic mice (db/db) were treated with placebo (vehicle) or DMOG (50 mg / kg) for 4 weeks. **(A)** There was no difference in blood glucose in *Lepr<sup>db/db</sup>* mice treated with placebo or DMOG (n = 7). **(B)** QPCR results demonstrate that DMOG increased the gene expression of HIF-1 target genes (n = 4–5). Data are shown as mean  $\pm$  SEM. ns = not significant. \*\*, p < 0.01; \*\*\*\*, p < 0.0001 analysed using unpaired two-sided Student's t-test. Source data are shown in **Figure 4—figure supplement 2—source data 1**.

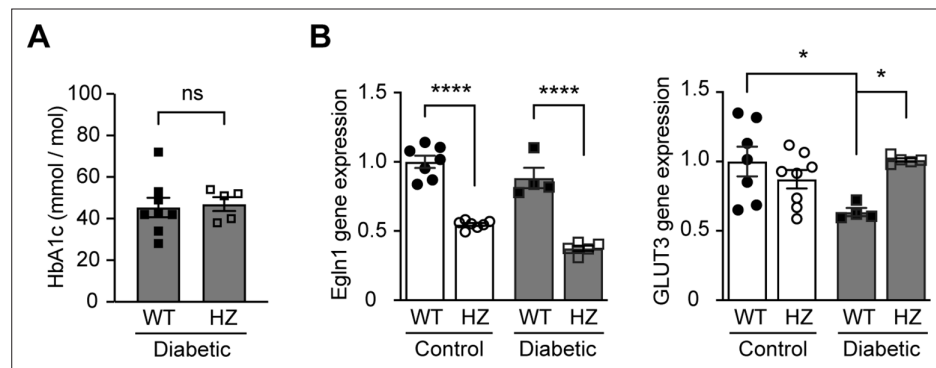


**Figure 4—figure supplement 3.** *Egln1* haplodeficiency increases HIF-1 target gene expression in diabetic mice without affecting blood glucose levels. *Egln1* haplodeficient (*Egln1*<sup>+/−</sup>, HZ) and corresponding Wild-type (WT) mice were induced diabetes using STZ. HbA1c (**A**) and gene expression (**B**) of *Egln1* and HIF-1 target gene *GLUT3* were assessed in non-diabetic control and diabetic WT and *Egln1*<sup>+/−</sup> mice (n = 4–8). Data are shown as mean ± SEM, and were analyzed using unpaired two-sided Student's t-test (**A**) and two-way ANOVA followed by Bonferroni's post hoc test (**B**). ns = not significant; \*, p < 0.05; \*\*\*\*, p < 0.0001. Source data are shown in **Figure 4—figure supplement 3—source data 1**.

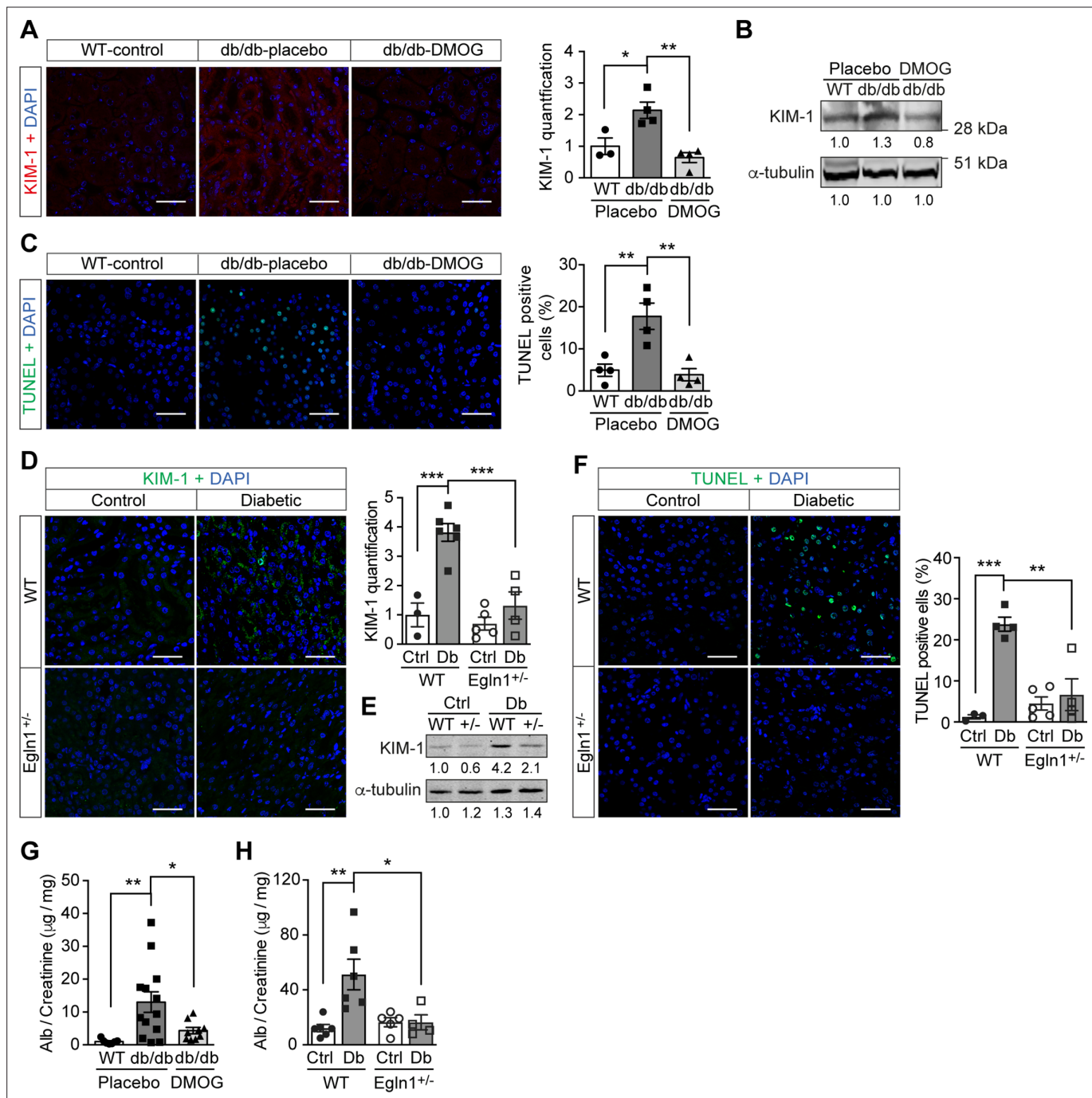


**Figure 5.** Promoting HIF-1 function reduces renal injury and ameliorates renal dysfunction in mouse models of diabetes. Kidneys were harvested from wild-type (WT) and *Lepr<sup>db/db</sup>* diabetic mice (db/db) that were treated with placebo (vehicle) or DMOG (**A–C, G**), and from non-diabetic control (Ctrl) or diabetic (Db) wild-type (WT) and *EglN1*<sup>+/-</sup> (+/-) mice (**D–F, H**). (**A and D**) Representative images of KIM-1 (red or green) and DAPI (blue) in kidney that were analysed using fluorescent immunohistochemistry. Quantifications of KIM-1 fluorescent signal are shown in corresponding histogram (**A**, n = 3–4; **D**, n = 3–6). (**B and E**) Representative images of KIM-1 and  $\alpha$ -tubulin analyzed by western blotting. (**C and F**) Apoptotic cells were detected using TUNEL staining, and the percentage of TUNEL-positive cells were quantified (**C**, n = 4; **F**, n = 3–5). (**G and H**) Albuminuria is presented as the ratio of albumin (Alb) to creatinine in mouse urine (**G**, n = 7–13; **H**, n = 4–6). Data are shown as mean  $\pm$  SEM. \*, p < 0.05; \*\*, p < 0.01; \*\*\*, p < 0.001 analysed using one-way ANOVA (**A, C**), Brown-Forsythe and Welch ANOVA (**G**) and two-way ANOVA (**D, F, H**) followed by multi-comparison test. Source data are shown in **Figure 5—source data 1**. Scale bar: 100  $\mu$ m.

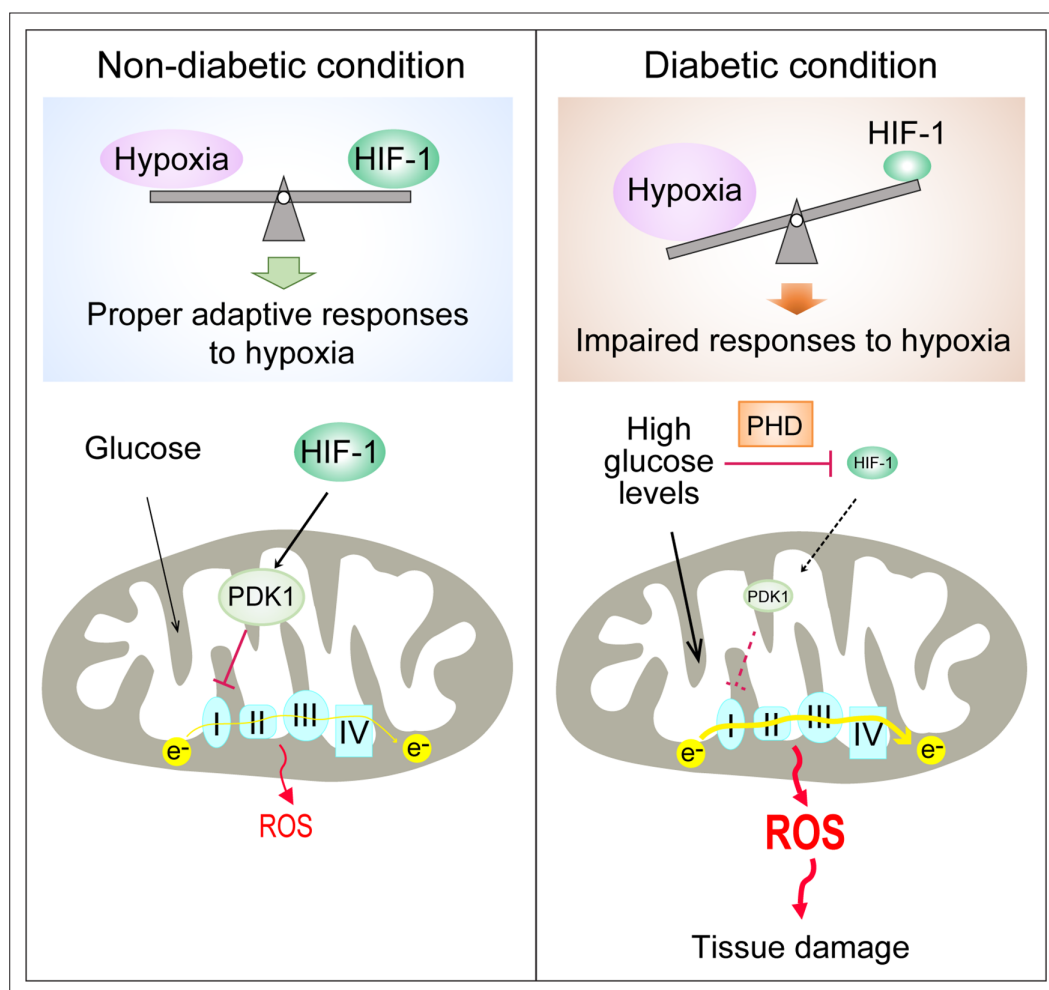


**Figure 6.** Repression of HIF-1 contributes to increased mitochondrial ROS production in diabetes. Under non-diabetic conditions (left panel), HIF-1 is induced by hypoxia and activates PDK1 expression which inhibits excess mitochondrial ROS production through inhibition of mitochondrial respiration. However, under diabetic conditions (right panel), HIF-1 is inhibited by high glucose levels through a PHD-dependent mechanism despite hypoxia. This results in decreased expression of PDK1, leading to increased mitochondrial respiration and excessive mitochondrial ROS production which causes tissue damage.